Z. Physik B 22, 49–58 (1975)

Raman Scattering Investigation of Ferroelastic Sb_5O_7I Crystals

W. Prettl
Physikalisches Institut der Universität Würzburg, Germany

K. H. Rieder
Max-Planck-Institut für Festkörperforschung, Stuttgart, Germany

R. Nitsche
Kristallographisches Institut der Universität Freiburg, Germany

Received May 13, accepted May 18, 1975

Abstract. Sb_5O_7I undergoes a displacive phase transition at 481 K where the symmetry is changed from C_{6h}^2 to C_{2h}^5. In the low temperature monoclinic phase the crystal is ferroelastic. The polarized Raman spectra of Sb_5O_7I have been measured at various temperatures below and above the phase transition. The frequencies and symmetries of most of the theoretically expected Raman active phonons in the ferroelastic phase have been determined. The observation of a soft mode in the ferroelastic phase which disappears above the phase transition together with the fact that the unit cell of the ferroelastic phase is twice as large as that of the paraelastic structure permits the conclusion that the phase transition results from a phonon instability at the Brillouin zone boundary M-point of the hexagonal phase. The temperature dependent splittings and intensity changes of several Raman lines are discussed with respect to the ferroelastic property of the crystal and the phase transition.

I. Introduction

Aizu has shown that a distinct class of crystals determined by symmetry may properly be called ferroelastics [1]. Ferroelasticity is most easily defined by its close analogy to ferroelectricity, where one has to replace the polarization by the strain and the electric field by the mechanical stress. The main difference is that in the ferroelastic phase a spontaneous tensorial quantity, the strain, arises instead of the polarization vector in the case of a ferroelectric. A ferroelastic crystal exhibits strain-stress hysteresis and has in the absence of an external stress two or more energetically equal orientational states (domains) of different spontaneous strain tensor. By a suitably chosen external stress the strain orientation may be shifted from one state to another.

By symmetry considerations Aizu found that among the nonmagnetic space groups there are 94 possible species of ferroelastic crystals and among these 52 are pure ferroelastic whereas the remaining 42 species are simultaneously ferroelastic and ferroelectric [1]. Up to now only few crystals are proved to be pure ferroelastic. One of these is Sb_5O_7I, which we will abbreviate in the following by SOI. SOI was synthesized recently by Krämer *et al.* [2]. In the present study we report Raman scattering measurements of SOI in the ferroelastic phase and discuss the spectra in view of

the symmetry of the crystal and the ferroelastic phase transition. The measurements have been performed below and above the transition temperature in the paraelastic phase. From the spectra as functions of temperature only those parts will be shown, which exhibit a significant change due to the ferroelastic property of the crystal and the phase transition.

II. Crystal Structure

In this section we will summarize the structural properties of SOI as far as it is necessary to discuss the Raman scattering spectra in the ferroelastic and in the paraelastic phase. Krämer has determined the crystal structure of SOI in both phases by X-ray diffraction [3]. Detailed structural parameters (e.g. atomic positions, lattice constants etc.) may by obtained from this reference.

In the paraelastic prototypic phase SOI belongs to the hexagonal system with space group $C_{6h}^2(P6_3/m)$. At 481 K SOI undergoes a displacive phase transition in the course of which the symmetry is reduced to $C_{2h}^5(P2_1/c)$ of the monoclinic system. Thus, according to the nomenclature of Aizu [1], SOI belongs to the full ferroelastic species $6/mF2/m$ having three orientational states of different spontaneous strain. The prototypic point group C_{6h} may be decomposed into the direct product $C_3 x C_{2h}$ where C_{2h} is the point group of the ferroic phase. This shows that the threefold rotations of C_3 transform one orientational state of the ferroic structure into another. In both phases SOI has a center of inversion.

In Fig. 1a a simplified projection of the crystal lattice on the monoclinic or hexagonal plane, respectively, is displayed. Only Sb- and I-atoms are shown on positions which they occupy in the ferroelastic structure*. A cartesian coordinate system which will be used throughout this paper is defined in Fig. 1b relating to the axes of the monoclinic and hexagonal elementary cell, $\vec{a}$, $\vec{b}$, $\vec{c}$ and $\vec{a}_1$, $\vec{a}_2$, $\vec{a}_3$, respectively. The cartesian z axis, $\vec{b}$ and $\vec{a}_3$ are oriented normal to the plane of Fig. 1.

The phase transition is characterized by a weak homogeneous distortion of the crystal lattice and an internal displacement of the atoms which yields a doubling of the unit cell. The average atomic displacements are of the order of 0.2 Å and the angle β (Fig. 1a) increases by 0.1° [3]. The internal distortion is mainly due to the displacements of the iodine atoms. In the hexagonal high temperature phase the unit cell contains two formula units Sb_5O_7I, where the iodine atoms are located one upon another along the $\vec{a}_3$ axis.

* This figure is obtained from Ref. 3. Note that the positions of the I-atoms are misprinted in this reference.

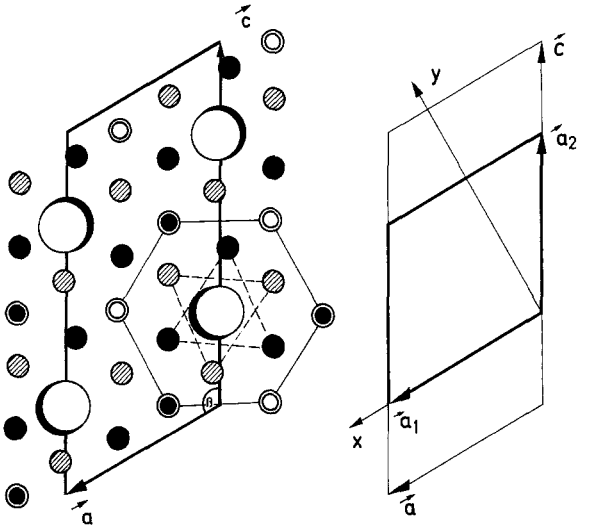

Fig. 1a and b. Structure of Sb_5O_7I. (a) Projection of the Sb- (small circles) and I-(large circles) atoms on the monoclinic plane. For the sake of clarity the O-atoms are omitted. Approximate heights z of the atoms given in units of a_3 normal to the plane of the drawing: *1* I: black/white: $z=0.00/0.50$, *2* Sb: black/lined: $z=0.25/0.75$, double circles black/white: $z=0.05/0.55$, double circles white/white: $z=0.45/0.95$. (b) Coordinate system. $\vec{a}_1$, $\vec{a}_2$ are hexagonal axes, $\vec{a}$ and $\vec{c}$ monoclinic axes, and x and y cartesian coordinates. The hexagonal $\vec{a}_3$ axis, the monoclinic $\vec{b}$ axis and the cartesian z-axis are normal to the figure

During the phase transition two equivalent I-atoms in neighbouring unit cells are translated alternately in opposite directions normal to the $\vec{a}_3$ axis. These displacements may take place along the three equivalent directions in the hexagonal structure $\pm\vec{a}_1$ (as shown in Fig. 1a) $\pm(\vec{a}_1+\vec{a}_2)/2$ and $\pm\vec{a}_2$ and thus, define the three ferroic domains as expected from the species $6/mF2/m$. Referring to the orientational state shown in Fig. 2a the unit cell is doubled along the $\vec{a}_2$ axis resulting in a monoclinic lattice which contains four formula units in the primitive cell. Because of the weak homogeneous deformation the basic periodicity vector $\vec{c}$ is now only approximately $2\vec{a}_2$.

III. Experimental

The measurements were performed using an argon laser as an exciting source, a Jarrel-Ash double monochromator to analyze the scattered radiation and an FW 130 photomultiplier as a detector. The optical resolution was 0.6 cm^{-1}. The direction of the polarization of the incoming laser beam could be selected by a broadband polarization rotator, that of the scattered radiation by a Polaroid filter.

The as-grown SOI crystals are optically transparent prisms with hexagonal cross sections. Samples of proper size were prepared by cleaving the crystals

perpendicular to the monoclinic $\vec{b}$ axis and grinding and polishing one hexagonal face parallel to a plane containing the $\vec{a}$ and $\vec{b}$ axis. By applying a small uniaxial stress on opposite hexagonal prism faces the samples were transformed into single domain crystals. The orientation of the sample may easily be determined by observing the extinction angles between crossed polarizers. The main vibrational directions of the optically biaxial crystal at room temperature include in the monoclinic plane an angle of 13° with the cartesian coordinate system defined in Fig. 1b. Basically this angle depends on wavelength (axial dispersion [4]) and on temperature. Therefore we have used as a reference frame for the polarization of the incident and the scattered light the cartesian coordinate system uniquely defined by the crystal structure.

The Raman polarizability tensors in the monoclinic phase are given by [5]:

$$\mathbf{P}(A_g)=\begin{pmatrix} P_{xx} & P_{xy} & 0 \\ P_{xy} & P_{yy} & 0 \\ 0 & 0 & P_{zz} \end{pmatrix}, \quad \mathbf{P}(B_g)=\begin{pmatrix} 0 & 0 & P_{xz} \\ 0 & 0 & P_{yz} \\ P_{xz} & P_{yz} & 0 \end{pmatrix}. \quad (1)$$

The incident beam was directed parallel to the z axis and the scattered radiation was observed in the usual 90° configuration, in y direction. The spectra were measured for the polarization configurations $z(xx)y$, $z(yx)y$, $z(xz)y$, and $z(yz)y$ referring to polarization directions outside the crystal. Inside the crystal the incident beam is weakly elliptically polarized due to the difference of the refractive index of the two optical main vibrational directions in the monoclinic plane. Thus, in general, the polarizability components P_{xx} and P_{xy} in the first two configurations and P_{xz} and P_{yz} in the last two configurations are mixed, however, both Raman active symmetries A_g and B_g are well separated as can be seen from (1). The spectra have been recorded at 100 K, at room temperature and at higher temperatures up to above the phase transition. The 100 K measurements were performed using a liquid nitrogen cooled cryostate. The temperature was determined from the intensities of Stokes and anti-Stokes scattering of several lines. For the measurements above room temperature the crystal was placed in an electrically heated oven with windows of fused quartz. The temperature was monitored by a NiCr – Ni thermocouple mounted close to the crystal and controlled by a Thor model 3010 temperature controller. A temperature stability of less than ±0.5 degrees could be achieved.

In order to avoid the formation of domains upon heating the crystal, the sample was stressed by a spring loaded piston in y direction against a small plate of fused quartz. The scattered radiation was observed through this quartz window. The applied uniaxial stress was adjusted to be slightly larger than the coercitive stress at room temperature.

IV. Raman Scattering Spectra of the Monoclinic Structure

a) Experimental Results

The Stokes Raman scattering spectra at 100 K are shown in Fig. 2 in the frequency range from 10 to 200 cm^{-1} and in Fig. 3 at higher frequencies. In order to make the intensities of the various records comparable the count rate of the peak intensity of one line is indicated in each spectrum. A large number of strong lines is observed at frequencies as low as 30 cm^{-1} up to 485 cm^{-1}. Besides these strong lines a lot of weak structures appear in the spectra. A very remarkable feature of the Raman scattering spectra is that, in particular at higher frequencies, many phonon lines of A_g symmetry coincide approximately or in some cases exactly within the limit of accuracy with

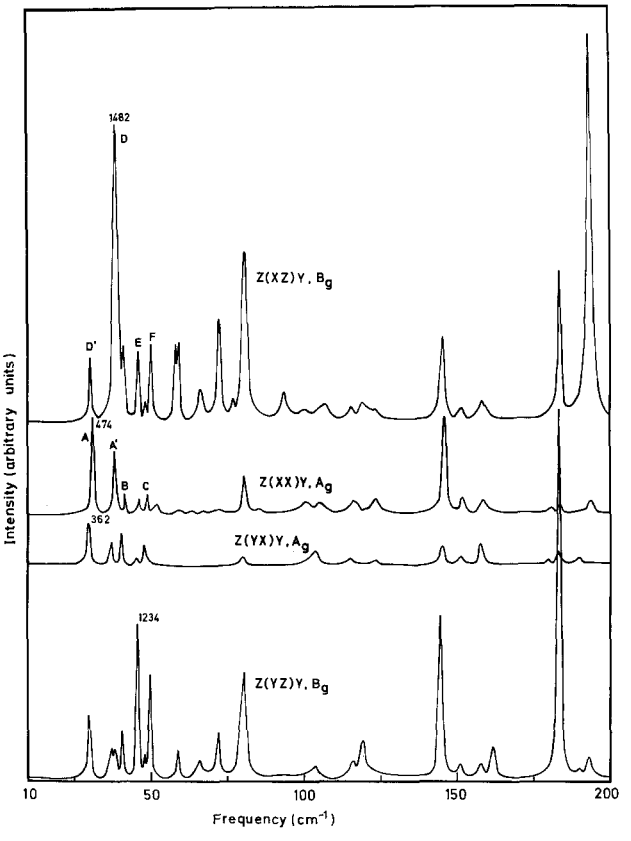

Fig. 2. Raman spectra of Sb_5O_7I in the ferroelastic phase at 100 K between 10 and 200 cm^{-1}. The numbers give the count rates for selected lines. The letters indicate lines, whose temperature dependence is shown in Fig. 6

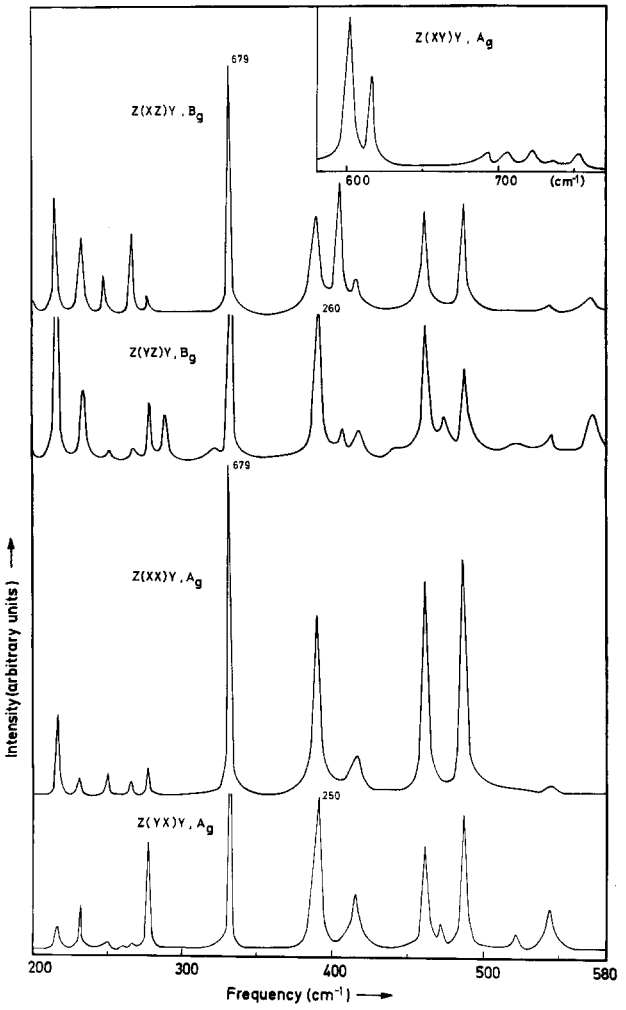

Fig. 3. Raman spectra of Sb_5O_7I in the ferroelastic phase at 100 K between 200 and 580 cm^{-1}. The numbers give the count rate for selected lines

Table 1. Experimentally determined frequencies (in wavenumbers) of Raman scattering lines of monoclinic Sb_5O_7I

Symmetry species: A_g		Symmetry species: B_g	
$T = 100$ K	$T = 300$ K	$T = 100$ K	$T = 300$ K
30	31	30	31
		38	40
37	39.5	41	–
41	41	46	45.5
48.5	–	48	–
79	79	50	48.5
100.5	–	58.5	–
104	104	59.5	57
105	–	66	–
115	110	72.5	70
123	–	80.5	80
145	145	93.5	–
151	–	100.5	–
157.5	156	104	–
216	210	107	–
231	231	115.5	–
250	–	119	111
265	–	123	–
276	272	145	145
330	330	151	–
390	387	158	–
415	–	161.5	–
460	456	183	182.5
470	–	193	190
486	478	215	212
543	334	233	232
705	–	248	–
723	–	267	–
751	–	247	–
		288	–
		331	–
		390	387
		405	–
		416	–
		460	455
		473	–
		486	478
		544	–
		571	568
		705	–
		723	–
		751	–

B_g symmetry lines. This cannot be caused by a misalignment of the crystal, as can be clearly seen at several parts of the spectra. For instance, at 183 cm^{-1} and 193 cm^{-1} there are two strong B_g lines in the $z(xz)y$ spectrum whereas the scattered intensity in the A_g spectrum of the $z(xx)y$ configuration is only 4% of the peak intensity of those lines (Fig. 2). This residual intensity is surely due to a not completely accurate orientation of the sample. Another clear separation of the spectra of different symmetries can be seen at 405 cm^{-1} (Fig. 3), where a rather strong line is found only in the $z(xz)y$ scattering configuration resulting from a B_g mode. A probable explanation of these coincidences will be deduced from compatibility relations among the space groups of both phases of SOI (see Chapter IV c).

Increasing the temperature to 300 K most of the weak lines disappear in the background. The stronger lines show the usual anharmonic frequency shift and broadening. A list of the frequencies and symmetry species of all Raman scattering lines measured at 100 K are given in Table 1. Totally we have found 28 lines due to phonons of A_g symmetry and 42 lines in the B_g spectra. The frequencies of those lines which are clearly observed at 300 K are also given in this Table 1.

b) Factor Group Analysis

The number of the Raman active phonons (as well as that of the infrared active and inactive phonons) and

Table 2. Factor group analysis of monoclinic Sb_5O_7I

$C_{2h}^5(P2_1/c)$			Numbers of irreducible representations			
Atom	Site symmetry	Wyckoff equipoint	Raman active		infrared active +acoustic	
			A_g	B_g	A_u	B_u
4 I	C_1	4 (e)	3	3	3	3
28 O			21	21	21	21
20 Sb			15	15	15	15
		Total	39	39	39	39

their distribution among the irreducible representations of the point group of the crystal can be determined by a factor group analysis. We will perform this analysis for the monoclinic structure and for the hexagonal phase though we have not measured completely the Raman spectra of the latter phase. The results dealing with the hexagonal structure will be required to establish compatibility relations in the next section.

As already mentioned Raman active phonons in the monoclinic phase belong to the symmetry species A_g and B_g of the point group C_{2h} whereas in the hexagonal structure Raman active modes transform according to the irreducible representations A_g, E_{1g} and E_{2g} of the point group C_{6h}. Knowing all atomic positions in the unit cell the factor group analysis is most easily accomplished by employing the tables of Adams and Newton [6]. In Tables 2 and 3 we have collected the data for both structures which enables us to decompose the total representation of the atomic displacements in the unit cell into irreducible representations. The first column gives the number of atoms occupying a site in the primitive cell of specific symmetry which is given in the second column. The third column indicates the Wyckoff notation [7] of this particular site preceded by the number of equivalent positions of this type of site in the unit cell. The following columns show how many times a set of equivalent atoms contributes to an individual irreducible representation. By summing up these columns we find the decomposition of the total representation of the prototypic phase Γ_p and of the ferroic phase Γ_f:

$$\begin{aligned}\Gamma_p &= 6A_g + 5E_{1g} + 7E_{2g} \quad \text{(Raman-active)}\\ &+ 6A_u + 7E_{1u} \quad \text{(infrared active)}\\ &+ 6B_g + 7B_u + 6E_{2u} \quad \text{(inactive)}\\ \Gamma_f &= 39A_g + 39B_g \quad \text{(Raman-active)}\\ &+ 38A_u + 37B_u \quad \text{(infrared active).}\end{aligned} \tag{2}$$

In both cases the representations of the translations of the crystal as a whole have been substracted. The decomposition for the ferroic phase may easily be proved. Each atom of this structure occupies a general 4-fold Wyckoff equivalent point (e) having the site symmetry C_1. Thus, the 12 vibrational degrees of freedom of a, group of four atoms on equivalent positions are distributed equally among the four irreducible representations of the point group C_{2h}. Furthermore it should be noted that in the hexagonal phase the dynamical displacements of the I-atoms do not contribute to any Raman active phonon (s. Table 3, first row) whereas, as stated above, in the monoclinic structure they may contribute to phonons of any symmetry species.

According to (2) the ferroelastic crystal should show 39 Raman active phonons of either symmetry species. Comparing this with the number of experimentally determined lines (Table 1) we see that we have found less lines of A_g symmetry but that there are three B_g modes more than theoretically expected to be Raman

Table 3. Factor group analysis of hexagonal Sb_5O_7I

C_{6h}^2 (P 6_3/m)			Numbers of irreducible representations							
Atom	Site symmetry	Wyckoff equipoint	Raman active			Infrared active +acoustic		Inactive		
			A_g	E_{1g}	E_{2g}	A_u	E_{1u}	B_g	B_u	E_{2u}
2 I	C_{3i}	2 (a)				1	1		1	1
2 O	C_{3h}	2 (d)			1	1	1	1		
4 Sb	C_3	4 (f)	1	1	1	1	1	1	1	1
6 Sb	C_s	6 (h)	2	1	2	1	2	1	2	1
12 O	C_1	12 (i)	3	3	3	3	3	3	3	3
		Total	6	5	7	7	8	6	7	6

active in first order. Since we have counted all observed Raman lines, among them some very weak structures, we suppose several of the weak lines to result from second order scattering. Thereupon we have also to attribute some of the weak lines in the A_g spectra to be due to two phonon scattering. Thus, more than 11 lines expected by the above symmetry considerations are missing in the A_g spectra. We note however that in general the scattering intensities of the A_g lines are considerably lower than those of the B_g lines.

c) Compatibility Relations

The appearance of the spontaneous strain together with the doubling of the unit cell in the course of the phase transition yields three essential implications for the Raman spectra. The spontaneous strain splits the double degenerate E_{1g} and E_{2g} modes and, in addition it may activate inactive modes of the center of the Brillouin zone. The doubling of the unit cell reduces the size of the Brillouin zone and shifts zone boundary modes into the center of the zone, thus further increasing the number of Raman active phonons. In Fig. 4 the cross section of the Brillouin zone normal to the sixfold axis of the hexagonal crystal or the twofold axis of the monoclinic lattice is shown. Various points of different symmetries in the Brillouin zone are designated by the usual symbols [8]. The doubling of one basic vector in the hexagonal plane yields the Brillouin zone to be folded normal to one Σ-axis. The zone boundary M-point is reflected to the zone center and the Brillouin zone becomes rectangular shaped. Thus, M-point phonons may become Raman active (or infrared active). The spontaneous strain further deforms the Brillouin zone yielding the typical cross section of a monoclinic cell. This is also displayed in Fig. 4, though it is strongly exaggerated for the sake of clarity.

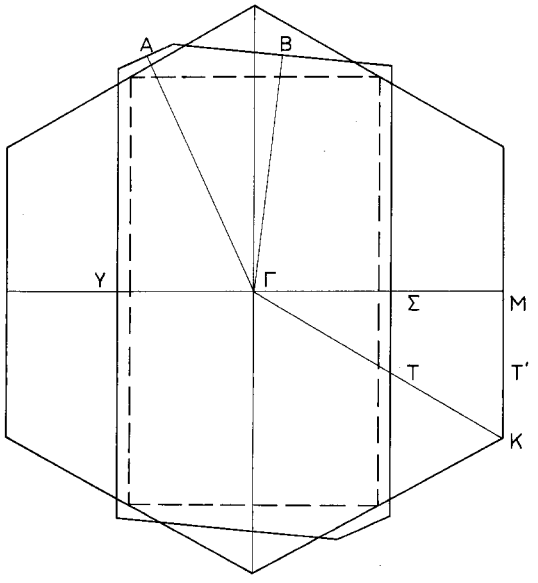

Fig. 4. Brillouin zone of Sb_5O_7I in the hexagonal and monoclinic phase. The symbols in the upper left quadrant characterize points of specific symmetries of the monoclinic phase whereas the symbols in lower right quadrant denote such points in the hexagonal phase. The broken line displays the zone resulting solely from the cell doubling

In order to determine the number and symmetry of the phonons in the monoclinic structure as they arise from the zone center and the zone boundary modes of the hexagonal phase, we have analyzed the compatibility relations along the Σ-axis in view of the reduction of the space group symmetry from C_{6h}^2 to C_{2h}^5. The results are shown in Table 4. The relations among the space group representations of C_{6h}^2 are summarized in the center of the table whereby the representations at the Σ-axis and the M-point are numbered in accordance with the tables of Zak [9]. The left and right hand columns give the irreducible representations at the zone center of the C_{2h}^5 structure as they result by reducing the symmetry. The correlations between the zone center modes (left side of the table) follow immediately from the frequently tabulated compatibility relations of the point groups [10]. The reduction of the zone boundary representations needs further consideration. Let us denote the factor group of the wave vector $\vec{\mathbf{q}}_M$ of C_{6h}^2 by G_M and that of $\vec{\mathbf{q}}=0$ of C_{2h}^5 by g_Γ. $\vec{\mathbf{q}}_M=(\vec{\mathbf{a}}_1\times\vec{\mathbf{a}}_3)\pi/V_h$ is the wave vector of the M-point, if we assume the unit cell to be doubled along the $\vec{\mathbf{a}}_2$ axis as shown in Fig. 1. V_h is the volume of the hexagonal unit cell. The symmetry elements of these groups and their representations are given in Table 5 [9]. The fractional translations are

$$\vec{\tau}_1=\vec{\mathbf{a}}_2=\vec{\mathbf{c}}/2$$
$$\vec{\tau}_2=\vec{\mathbf{a}}_3/2=\vec{\mathbf{b}}/2. \tag{3}$$

Both factor groups are isomorphic to the point group C_{2h}. Thus, we have labelled the representations of g_Γ by the usual point group notations and have appended these notations to the corresponding irreducible representations M_i of G_M. The symmetry elements of g_Γ differ from those of G_M by the translation $\vec{\tau}_1$ which is a fractional translation of C_{2h}^5 and a primitive translation of C_{6h}^2. Consequently, in order to determine how the M_i modes are transformed by the symmetry operations of g_Γ, we have to multiply the representations of the operations containing C_2 and σ_z by the factor $\exp\{\vec{\tau}_1\cdot\vec{\mathbf{q}}_M\}=-1$. Keeping the table of characters unchanged this yields a rearrangement of the order

Table 4. Compatibility relations of the normal modes along the Σ-axis of the hexagonal C_{6h}^2-phase with respect to the reduction of the symmetry to C_{2h}^5. The central part of the table shows the relations among the symmetry species of C_{6h}^2. The compatibility of Γ-point and M-point representations of C_{6h}^2 with Γ-point representations of C_{2h}^5 is given at the right and left side

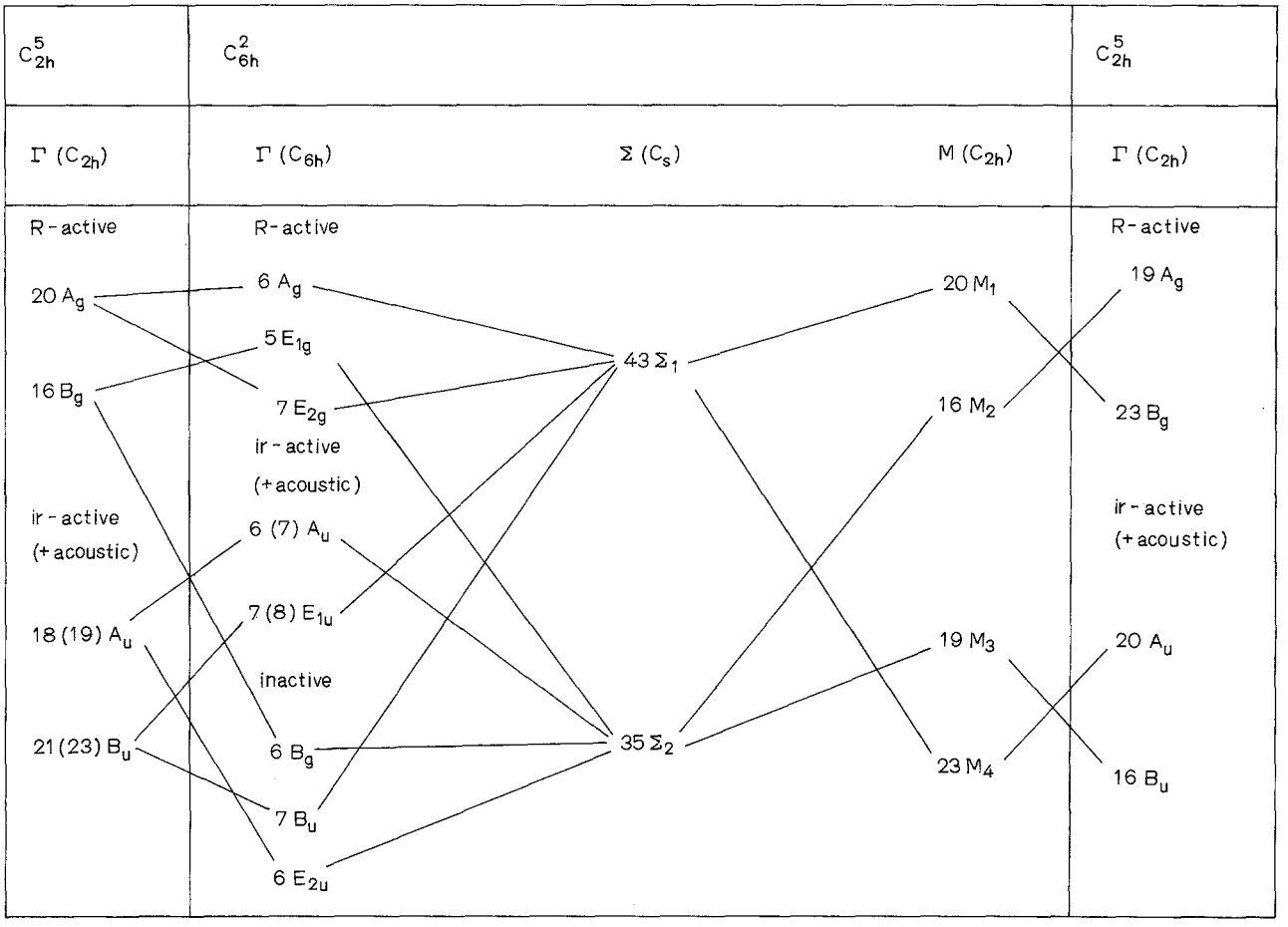

Table 5. Irreducible representations of G_M and g_Γ

G_M		E	I	$\{C_2/\tau_2\}$	$\{\sigma_z/\tau_2\}$
	g_Γ	E	I	$\{C_2/\tau_1+\tau_2\}$	$\{\sigma_z/\tau_1+\tau_2\}$
$M_1(A_g)$	$(M_2)A_g$	1	1	1	1
$M_2(B_g)$	$(M_1)B_g$	1	1	−1	−1
$M_3(A_u)$	$(M_4)A_u$	1	−1	1	−1
$M_4(B_u)$	$(M_3)B_u$	1	−1	−1	1

of the M_i given in parenthesis in the columns of the irreducible representations of g_Γ. Thus, the desired compatibility relations follow directly by attaching the M_i to the corresponding representation of g_Γ of the same line in Table 5.

From these relations we may obtain the symmetry species of both $\mathbf{\hat{q}}=0$ phonons in the monoclinic structure which originate from the $\mathbf{\hat{q}}=0$ and the $\mathbf{\hat{q}}_M$ mode of the same optical phonon branch of the hexagonal phase. It is found that, if both endmembers of an optical branch of the hexagonal phase yield Raman active phonons in the lower symmetry structure, one of these phonons belongs to the A_g species the other is a B_g mode. They never transform according to the same irreducible representation. This result seems to explain the fact that several Raman lines due to A_g and B_g phonons approximately coincide in frequency. Since SOI has many atoms in the unit cell, we may assume that the higher optical branches are flat. Therefore, the zone center and zone boundary phonons of the same branch differ only slightly in frequency.

V. Phase Transition

Increasing the temperature above the phase transition several line splittings are removed and the intensities

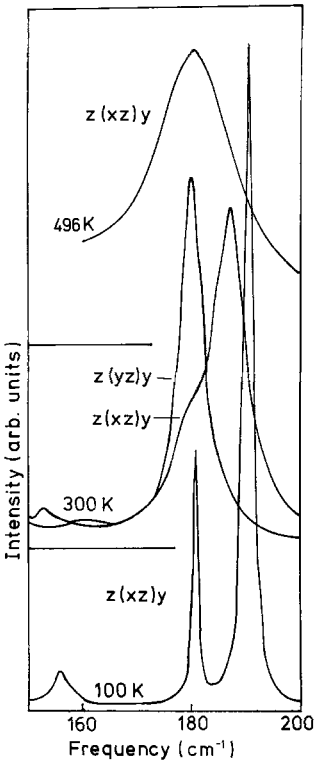

Fig. 5. Splitting of an E_{1g} doubly degenerate mode of the hexagonal structure into two B_g phonons in the monoclinic phase. For 300 K two polarization configurations are plotted in order to show the splitting clearly

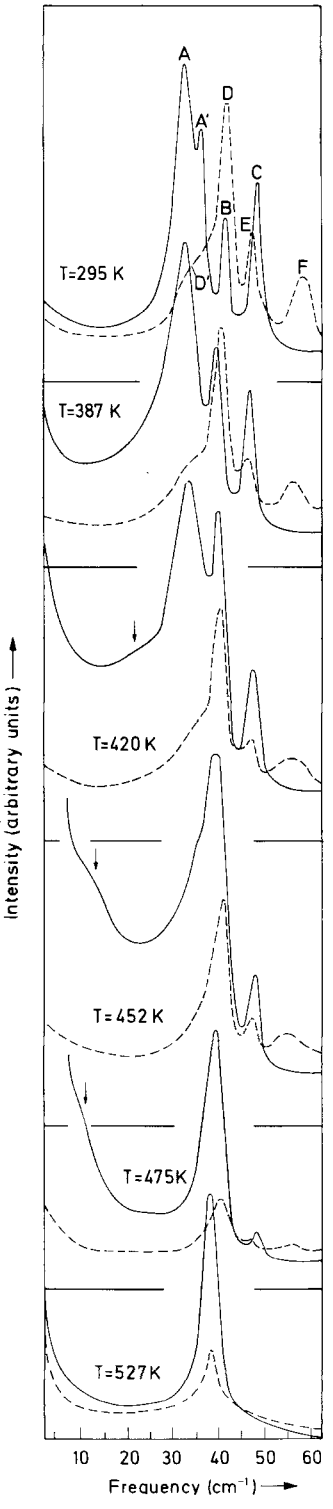

Fig. 6. Temperature dependence of low frequency Raman lines below and above the phase transition at $T_c = 481$ K. Full line: A_g, $z(xx)y$, broken line: B_g, $z(xz)y$

of many lines become strongly temperature dependent and disappear as the transition point is approached. One example for two lines converging with increasing temperature is shown in Fig. 5. The splitting of two B_g modes of the monoclinic structure is removed as the spontaneous strain vanishes yielding one E_{1g} species phonon of the hexagonal phase.

The most significant changes of line intensities with temperature have been found in the very low frequency part of the spectra, below 60 cm^{-1}. This is displayed in Fig. 6. At 295 K there are four A_g lines: A, A', B, C and four B_g lines: D, D', E, F. These lines are also indicated by the same letters in the spectra of Fig. 2 which are measured at 100 K. At 295 K the lines A and A' are close together, and D' can only be observed as a shoulder of line D. However, at 100 K these lines are well separated as can be seen in Fig. 2. Raising the temperature the intensities of the lines C, E and F decrease continuously and they disappear at the transition temperature. The line A' decreases in frequency and cannot be separated from line A at 387 K. At higher temperatures a weak shoulder ap-

pears at the low frequency side of A (see 420 K record). Further raising the temperature increases the scattering intensity in the valley between the Rayleigh line and the line A of the A_g spectrum strongly in contrast to the B_g spectrum. At 452 K a weak and broad line which vanishes at the transition temperature appears in the wing of the Rayleigh line. Above the phase transition both the rather high intensity and the large width of the Rayleigh line in the A_g spectrum decrease to a magnitude comparable with that of the B_g spectrum. The A_g lines A and B and the B_g lines D and D' run together becoming doubly degenerate E_{2g} and E_{1g} modes, respectively, of the hexagonal phase.

The peculiar behaviour of the scattering intensity at very low frequencies of the A_g spectrum seems to be explained best by assuming a rather strongly damped soft mode being split off from the A, A' doublet. Having the same symmetry both modes interact, whereby the higher frequency component is stabilized at almost the original frequency and the lower frequency component becomes soft. During the interaction the intensity is exchanged between both lines. Similar mode coupling situations have been observed in other crystals with phase transition [11, 12]. In Fig. 6 we have indicated the broad line due to the soft mode by arrows.

Above the phase transition the A_g soft mode may belong to the representations A_g, E_{2g} or M_2 of C_{6h}^2 (see Table 4). In the first two cases this mode should be Raman active. Since we have not observed a soft mode in the Raman spectrum of the hexagonal phase we assume that the last case is realized. Therefore we conclude that the structural instability of the hexagonal phase of SOI is induced by a zone boundary soft mode having the symmetry M_2. This conclusion is supported by the fact that it explains in a natural way the doubling of the unit cell in the low temperature phase. Thus, the ferroelasticity of SOI results from anharmonic coupling of a M_2-phonon with elastic deformations (long wavelength acoustic phonons), rather than from a zero wavenumber Raman active soft mode in the prototypic phase or an elastic instability as it occurs in "normal" ferroelastics [13]. In this sense SOI is comparable with $Gd_2(MoO_4)_3$ and related crystals, whose ferroelectric and ferroelastic properties are induced by an instability of a doubly degenerate zone boundary mode [14–16].

The Raman scattering of the lines C, E and F, which vanish when approaching the phase transition from below is induced by the spontaneous strain (B_g modes) and/or the frozen displacements of the M_2-soft mode. It can be shown that the intensity of such a line is proportional to the square or the fourth power of the soft mode amplitude depending whether the corresponding phonon has the wave vector $\vec{q}_M$ or $\vec{q}=0$ in the hexagonal phase, respectively [17]. As we have to regard the soft mode amplitude in the ferroic phase to be the order parameter of the phase transition, the experimentally found continuous decrease of the intensities of the lines C, E and F suggests the conclusion that the phase transition of SOI is of second order. This conclusion is confirmed by DTA measurements of Krämer [18]. However, since close to the transition temperature the measured intensities of these lines are very low and, thus, rather inaccurate, the order of the phase transition cannot finally be determined by Raman measurements alone. But we can say that, in the case the phase transition is of first order, the jump of the order parameter at T_c must be rather small.

As we have shown in Chapter IV b, the iodine atoms do not contribute to any Raman active phonon in the hexagonal phase, but they do in the monoclinic structure. These results together with the fact that the iodine atoms are the heaviest atoms in the SOI lattice which justifies the assumption that they play a role essentially in low frequency modes seem to explain that the most strongly temperature dependent Raman lines appear at very low frequencies. The intensities of the lines C, E and F reflect in some way the displacements of the iodine atoms from their equilibrium position of the hexagonal phase. A quantitative discussion along this line relating the temperature dependence of these modes to a phenomenological thermodynamic potential describing the phase transition will be the subject of a subsequent paper [17].

The authors are indebted to Dipl.-Phys. M. Schuhmacher and Dr. V. Krämer for providing the crystals and communicating their results on the properties and the structure of the crystals before publication. One of the authors (W.P.) wishes to express his gratitude to Professor H.G. Häfele for his encouragement and continuous interest in this work. Financial support by the Deutsche Forschungsgemeinschaft is gratefully appreciated.

References

1. Aizu, K.: J. Phys. Soc. Japan **27**, 387 (1969)
2. Krämer, V., Nitsche, R., Schuhmacher, M.: J. Cryst. Growth **24/25**, 179 (1974)
3. Krämer, V.: Acta Cryst. B **31**, 234 (1975)
4. Born, M., Wolf, E.: Principles of Optics, 5th ed. Oxford: Pergamon Press 1975
5. Loudon, R.: Adv. Phys. **13**, 423 (1967)
6. Adams, D.M., Newton, D.C.: Tables for Factor Group and Point Group Analysis. Cryodon (England): Beckmann-RIIC Limited 1970
7. Wyckoff, R.W.G.: Crystal Structures, vol. 1. New York: Interscience 1948

8. Koster, G.F.: Solid State Physics, vol. 5, pp. 173–256. New York: Academic Press 1957
9. Zak, J.: The Irreducible Representations of Space Groups. New York: Benjamin 1969
10. Fateley, W.G., Dollish, F.R., Devitt, N.T., Bentley, F.F.: Infrared and Raman Selection Rules for Molecular and Lattice Vibrations. New York: Wiley-Interscience 1972
11. Steigmeier, E.F., Harbeke, G., Wehner, R.K.: Proc. 2nd Internat. Conf. Light Scattering in Solids, pp. 396–400. Paris: Flammarion 1971
12. Scott, J.F.: Rev. Mod. Phys. **46**, 83 (1974)
13. Aizu, K.: J. Phys. Chem. Solids **32**, 1959 (1971)
14. Aizu, K.: J. Phys. Soc. Japan **33**, 629 (1972)
15. Aizu, K.: J. Phys. Soc. Japan **31**, 802 (1971)
16. Dvořák, V.: Phys. Stat. Sol. (b) **45**, 147 (1971)
17. Prettl, W., Rieder, K.H.: To be published
18. Krämer, V.: Private communication

Dr. W. Prettl
Physikalisches Institut der Universität
D-8700 Würzburg
Röntgenring 8
Federal Republic of Germany

Dr. K.H. Rieder
Max-Planck-Institut für Festkörperforschung
D-7000 Stuttgart 1
Heilbronner Straße 69
Federal Republic of Germany

Professor Dr. R. Nitsche
Kristallographisches Institut der Universität
D-7800 Freiburg
Hebelstraße 25
Federal Republic of Germany